Plane-wave dynamics of optical parametric oscillation with simultaneous sum-frequency generation

Gülbin Akgün, Yamaç Dikmelik, and Orhan Aytür

Department of Electrical and Electronics Engineering, Bilkent University, TR-06533 Bilkent, Ankara, Turkey

Phone: 90-312-266-4307; Fax: 90-312-266-4126; e-mail: aytur@ee.bilkent.edu.tr

Single-crystal upconversion optical parametric oscillators (OPO's) where either second-harmonic[1] or sum-frequency[2] generation is simultaneously phase-matched with parametric generation have recently been demonstrated. Here, we present the plane-wave dynamics of simultaneous parametric oscillation and sum-frequency generation (SFG), where the resonant OPO signal field is summed with the pump field. Our analysis presumes that simultaneous phase-matching of the SFG and OPO processes has been achieved utilizing birefringent phase matching (BPM). However, quasi phase-matching either or both processes is another promising possibility, and our results can readily be extended to those cases.

Potential polarization geometries for collinear BPM shown in Fig. 1 lead to four different sets of coupled mode equations depending on which field components are common to the two processes inside the crystal. We designate these sets as classes A through D. Some of these geometries require the polarization of certain fields to be rotated in order to have components along both fast and slow axes of the nonlinear crystal.

The absence of idler and sum frequency fields at the input of the crystal makes it possible to reduce the coupled mode equations for the complex field amplitudes to a set of equations for real variables a_m in all classes. We normalize the fields so that $\phi_m = a_m^2$ represent the photon flux densities.

Polarization geometries where no polarization rotation is required and the signal and pump fields have contributions from both OPO and SFG processes belong to class A. The equations describing this interaction are

$$\frac{da_i}{dz} = \kappa_a a_s a_p \tag{1}$$

$$\frac{da_s}{dz} = \kappa_a a_i a_p - \kappa_b a_p a_{sf} \tag{2}$$

$$\frac{da_p}{dz} = -\kappa_a a_i a_s - \kappa_b a_s a_{sf} \tag{3}$$

$$\frac{da_{sf}}{dz} = \kappa_b a_s a_p, \tag{4}$$

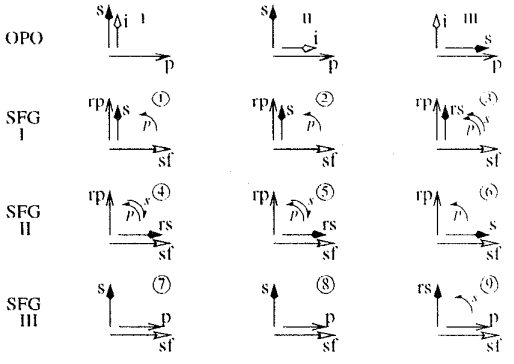

Figure 1: Polarization geometries leading to simultaneous phase-matching.

0-7803-4950-4/98/$10.00 1998 IEEE

where

$$\kappa_a = d_e \sqrt{\frac{2\hbar}{c^3 \epsilon_0}} \sqrt{\frac{\omega_i \omega_s \omega_p}{n_i n_s n_p}} \tag{5}$$

is the coupling constant of the OPO process. Here, d_e denotes the effective nonlinear coefficient, the frequencies are related by $\omega_p = \omega_i + \omega_s$, and n_m are the corresponding refractive indices. The coupling constant κ_b is defined similarly for SFG. The ratio $\beta = \kappa_b / \kappa_a$ is an important quantity determining the relative strengths of the two processes. The nonlinear drive, $D = \phi_p(0)\ \kappa_a^2 l^2$, for a crystal of length l is a measure of how strongly the device is pumped.

Using the proportionality of Equations (1) and (4), class A equations can be reduced to those of an ordinary OPO, and the solutions can be expressed in terms of Jacobi elliptic functions.

We investigate the temporal evolution of the OPO by simulating the growth of the intracavity signal from noise similar to the analysis of OPO's with intracavity SFG crystal.[3] As a measure of performance, we evaluate the photon conversion efficiency (twice the ratio of sum frequency photon flux at the crystal output to input pump photon flux).

For nonlinear drive values below threshold, there is no conversion. Above threshold, a well-defined steady state, multistability, periodicity or chaotic behaviour can be observed depending on the values of various parameters.

For class A devices, if β is larger than unity, the signal is not amplified for any value of the nonlinear drive and there is no oscillation. As β increases towards unity, maximum conversion efficiency increases. Depending on the value of the nonlinear drive, single or multiple steady states are observed (see Fig.2). β is closely related to natural properties of the crystal, therefore, it is not adjustable. Nevertheless, crystals with β larger than unity can be found.

Class B has no field components common between the OPO and SFG processes and therefore requires polarization rotations before the cavity for the pump and inside the cavity for the resonant signal fields. The fields evolve according to well known OPO and SFG solutions.

Class C requires a polarization rotation of the pump field. The rotation angle α is another important parameter. The signal field which couples the two processes is amplified by OPO and attenuated by SFG. The equations governing the behaviour of class C signal, pump and rotated pump fields are

$$\frac{da_s}{dz} = \kappa_a a_i a_p - \kappa_b a_{rp} a_{sf} \tag{6}$$

$$\frac{da_p}{dz} = -\kappa_a a_i a_s \tag{7}$$

$$\frac{da_{rp}}{dz} = -\kappa_b a_s a_{sf}. \tag{8}$$

Analytical solutions for these classes are not available, hence, we used Runge-Kutta integration to calculate single pass solutions. Small signal gain of a class C device is given by

$$g = \cosh^2 \left(\cos\alpha \sqrt{1 - \beta^2 \tan^2 \alpha}\ \kappa_a a_p(0)\ l \right) \tag{9}$$

with the requirement that $\beta \tan\alpha < 1$ for the oscillation to start. For α and β values satisfying this condition a threshold value for the nonlinear drive can be determined.

For class C, above the threshold nonlinear drive value, first steady oscillation is observed. For some α and β values, as the nonlinear drive increases further, transition to chaos through period doublings occurs (see Fig.3). Increasing α brings an increase in conversion efficiency, but causes chaos to start at smaller nonlinear drive values.

In class D, the signal field requires an intracavity polarization rotation and the pump field provides the coupling. The rotation angle α can be optimized for particular values of the nonlinear drive and β to maximize the conversion efficiency (See Fig.4).

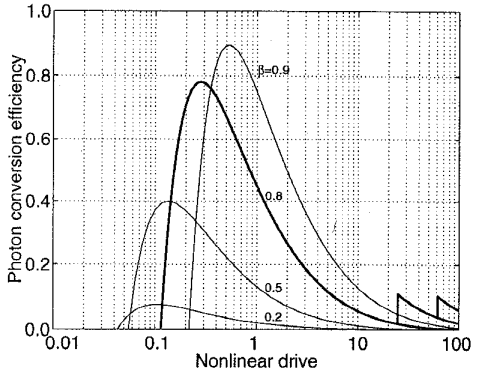

Figure 2: Photon conversion efficiency as a function of the nonlinear drive in class A OPO's for various values of β. Multistability is displayed for the $\beta = 0.8$ case only.

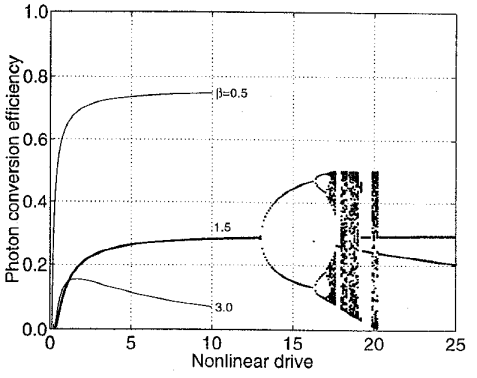

Figure 3: Photon conversion efficiency as a function of the nonlinear drive in class C OPO's with $\alpha = 45.9°$ for $\beta = 0.5$, $\alpha = 30°$ for $\beta = 1.5$, and $\alpha = 16.2°$ for $\beta = 3$.

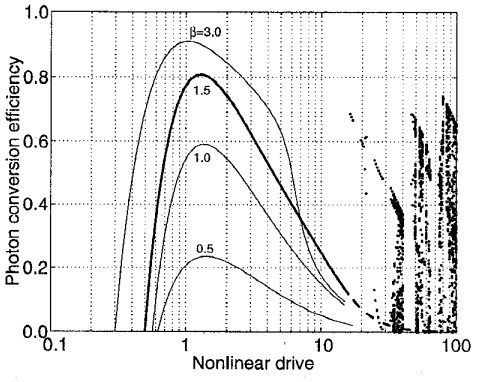

Figure 4: Photon conversion efficiency as a function of the nonlinear drive in class D OPO's for various values of β. In each case, α is adjusted to maximize the conversion efficiency at a nonlinear drive of 1, yielding $\alpha = 39.7°$ for $\beta = 0.5$, $\alpha = 38.1°$ for $\beta = 1$, $\alpha = 35.9°$ for $\beta = 1.5$, and $\alpha = 27.8°$ for $\beta = 3$. The chaotic regime is displayed for the $\beta = 1.5$ case only.

In conclusion, we classified the single-crystal upconversion OPO's with simultaneous SFG and investigated their plane-wave dynamics. Our results show that classes A and D are efficient frequency upconverters. The performance of class A OPO's is limited by crystal properties whereas classes C and D can be optimized by adjusting the polarization rotation angle.

1. T. Kartaloğlu, K. G. Köprülü, and O. Aytür, Opt. Lett. **22**, 280 (1997).
2. K. G. Köprülü, T. Kartaloğlu, and O. Aytür, in *Conference on Lasers and Electro-Optics*, Vol. 11 of OSA Technical Digest Series (Optical Society of America, Washington, D.C., 1997) p. 457.
3. G. T. Moore and K. Koch, IEEE J. Quantum Electron. **29**, 961 (1993).
4. O. Aytür and Y. Dikmelik, to be published in IEEE J. Quantum Electron. **34**, March 1998.